AIAA JOURNAL
Vol. 40, No. 3, March 2002

Residual Strength Prediction of Aircraft Fuselages Using Crack-Tip Opening Angle Criterion

Chuin-Shan Chen,* Paul A. Wawrzynek,† and Anthony R. Ingraffea‡
Cornell University, Ithaca, New York 14853

Ductile tearing simulation and residual strength prediction of wide-body, lap-jointed fuselage panels are conducted. The damage configurations of the fuselage panels consist of a single lead crack and a lead crack with small multiple-site damage (MSD). The crack-tip opening angle fracture criterion and elastic-plastic finite element analysis are used to control stable crack advancement under conditions of general yielding. Thin-shell finite elements are used to model the fuselage structures except in the vicinity of cracks. In this region special plane-strain shell elements are used to capture three-dimensional constraint effects during stable crack growth. A global-local modeling procedure is employed in the numerical analyses. We show that accurate representation of the load transfer through the rivets is crucial for the stress distribution prediction. Modeling fatigue crack closure is essential to capture the fracture behavior at ductile tearing initiation. Breakage of a tear strap can have a major influence on residual strength prediction. Predicted crack growth and residual strength considering fatigue crack closure and tear strap failure agree reasonably well with test results. Observed and predicted results both indicate that the occurrence of small MSD cracks substantially reduces the residual strength.

I. Introduction

MODERN aircraft structures are designed using a damage tolerance philosophy.[1] This philosophy envisions sufficient strength and structural integrity of the aircraft to sustain major damage and to avoid catastrophic failure in the presence of discrete source damage. However, as the aircraft is operated beyond its original design life, simultaneous presence of small fatigue cracks at adjacent structural details might occur. Such a damage scenario, known as multiple-site damage (MSD), might be too small to be detected and can lead to a catastrophic failure in flight.[2] Concern for the safety of aging aircraft prompts the development of a reliable methodology for simulating stable crack growth and predicting residual strength of pressurized fuselages with MSD. An accurate and reliable analysis methodology allows engineers to maintain aging aircraft economically while ensuring continuous airworthiness. Consequently, it improves the technology to support the safe operation of the current aircraft fleet as well as the design of more damage-tolerant aircraft for the next generation fleet.

In recognition of the need, NASA initiated the Airframe Structural Integrity Program (ASIP)[3] to develop advanced analysis methodologies for assessing damage tolerance of aging aircraft. The work presented in this paper is part of the developments under the ASIP program. The goal is to develop a computational analysis methodology to predict residual strength of built-up aircraft fuselages.

The behavior of lead and MSD cracks in fuselage structures is mainly dominated by bulging and plasticity effects.[4] Structures with bulging, or out-of-plane deformation at crack edges caused by pressure loading, typically undergo large displacements and rotations. To model this behavior, large deformation analysis that establishes the nonlinear equilibrium state of structures in an unknown, deformed configuration is required. Formulations for uncracked stiffened thin shells are well developed, and general finite element programs are capable of handling this class of problem. The readers are referred to Ref. 5 for more in-depth discussion of such formulations.

Plasticity effects in the vicinity of crack tips play a key role in characterizing fracture processes in thin-sheet metallic structures. Various methods have been developed over the past few decades to predict crack growth in metals. However, for thin-sheet materials exhibiting a large amount of plasticity and stable crack growth prior to failure there is no consensus on the most satisfactory method.[6,7] Two common fracture parameters exist in the literature, the J integral and the crack-tip opening angle (CTOA).[8,9] The J integral is known to be an effective parameter to characterize the intensity of the near-tip stress and deformation fields for stationary cracks subjected to monotonic loadings but loses its significance as a crack-tip parameter for extended amounts of crack growth accompanied by elastic unloading.[9] Recently, the T_ϵ^* integral has been developed to characterize the energy dissipated in such cases.[10]

The CTOA fracture criterion has long been recognized as a viable fracture parameter for modeling stable crack propagation in ductile materials.[9] The CTOA criterion is a local fracture parameter assuming that the near-tip plastic strains, thus the near-tip displacements, in the vicinity of a crack control fracture. Comparisons between the energetic approach (J and T_ϵ^*) and the CTOA approach can be found in Refs. 11 and 12. The CTOA fracture criterion has been successfully applied to predict residual strength of thin-sheet aluminum flat panels[13,14] and will be used for subsequent simulations in this study.

Built-up lap-jointed aircraft fuselages, consisting of skins, tear straps, stringers, frames, and stringer clips, are geometrically complicated and innately three-dimensional. Modeling crack growth processes inevitably increases this complexity. In this study a software system FRANC3D/STAGS has been developed to model the fracture processes in aircraft structures[15,16] [data also available online at www.cfg.cornell.edu (cited 1 July 2000) for the Cornell Fracture Group, FRANC3D Version 1.14 Thin Shell Tutorial Guide (DRAFT)]. The program is capable of tracing geometry evolution during crack growth using FRANC3D[17] and performing nonlinear thin shell analysis using STAGS.[18]

The paper is organized as follows. In Sec. II recent developments of the CTOA fracture criterion for residual strength prediction are reviewed. Full-scale wide-body fuselage panel tests used to validate the criterion and software being developed are briefly outlined in Sec. III. Finite element models for crack growth analysis in lap-jointed fuselage panels are presented in Sec. IV. Calibration of the critical CTOA ($CTOA_c$) from laboratory flat panel tests are described. Calculated stress distributions are compared with strain gauge readings in Sec. V. Comprehensive comparisons between

Received 18 August 2000; revision received 13 July 2001; accepted for publication 13 July 2001.

*Research Associate, The Cornell Fracture Group; currently Assistant Professor, Department of Civil Engineering, Rm. 312, National Taiwan University, 1, Roosevelt Road, Sec. 4, Taiwan 10617, Republic of China.

†Senior Research Associate, The Cornell Fracture Group, 641 Rhodes Hall.

‡Dwight C. Baum Professor of Engineering, The Cornell Fracture Group, 641 Rhodes Hall.

predicted and measured crack growth and residual strength are presented in Sec. VI.

II. CTOA Fracture Criterion

The CTOA fracture criterion is based on crack-tip opening displacement (CTOD) concept proposed by Wells.[19] Because the CTOD has a limiting value of zero at the crack tip, the local slope of the crack-tip opening profile, or CTOA, was suggested to characterize the crack growth behavior.[20,21] Newman,[22] Rice and Sorensen,[23] and Kanninen and Popelar[9] further defined the CTOA as the CTOA measured at a fixed distance behind the moving crack tip.

The CTOA fracture criterion asserts that the angle maintains a constant value during stable crack growth for a given thickness of a metallic material. The definition of CTOA as suggested by Newman[22] is adopted. For Mode-I only deformations it is defined as (Fig. 1)

$$\text{CTOA} = 2\tan^{-1}(\delta/2d) \tag{1}$$

where δ is the CTOD measured at a specific distance d behind the crack tip. For mixed-mode problems the opening angle is obtained from the cross product of two vectors:

$$\text{CTOA} = \sin^{-1}\frac{\|\boldsymbol{a}\times\boldsymbol{b}\|}{\|\boldsymbol{a}\|\,\|\boldsymbol{b}\|} \tag{2}$$

where $\boldsymbol{a}$ and $\boldsymbol{b}$ are the vectors from the crack tip to crack edges at a specific distance d behind the crack tip.

Previous studies for residual strength prediction using two-dimensional elastic-plastic analyses reached a mixed degree of success.[22] Typically, the predicted residual strength would agree with test results up to a certain width of the panels. The discrepancy between two-dimensional predictions and test results for larger panels was determined to be related to the three-dimensional constraint effects. Although thin-sheet structures behave essentially in plane stress, the constraint caused by the finite thickness of the specimens can cause the regions local to the crack tip to approach plane-strain conditions.[24–26] The observation can be also inferred from the microscopic behavior because ductile fracture of metals is basically a result of microvoid nucleation, growth, and coalescence.[27] Thus, the main parameters control fracture are plastic strains (or CTOA) and stress triaxiality (constraint).

Extensive numerical studies of two- and three-dimensional elastic-plastic fracture analyses have been conducted to investigate the constraint effects on residual strength prediction.[25,28–30] From these studies it has been concluded that although three-dimensional simulations are ideal to quantify the constraint effects, two-dimensional simulations with the plane-strain core concept (Fig. 2) seem adequate to assess residual strength prediction. We adopt the plane-strain core concept for the subsequent thin-shell finite element analyses.

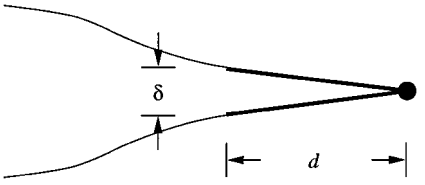

Fig. 1 Illustration of CTOA definition.

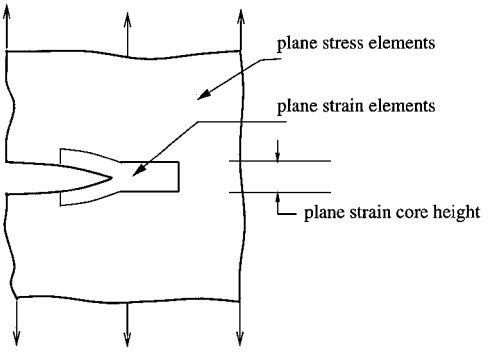

Fig. 2 Schematic of the plane-strain core.

III. Full-Scale Fuselage Panel Testing

The full-scale fuselage panel tests investigated in this study were performed on a wide-body pressure test fixture with a radius of curvature of 127 in. (3226 mm). The tests, funded by the Federal Aviation Administration (FAA) and performed by the Boeing Commercial Airplane Group, were intended to characterize crack growth in a generic wide-body, lap-jointed fuselage configuration subjected to MSD. A brief overview of the panel tests is presented next. More information about the fixtures and tests can be found in Refs. 31–34.

Two identical curved lap-jointed panels were fabricated. The test panels were designed to simulate typical wide-body fuselage crown structures consisting of bonded tear straps and floating frames connected to hat section stringers with stringer clips. Skins and tear straps were made of 0.063-in. (1.6-mm)-thick, 2024-T3 clad aluminum alloy. Stringers, frames, and stringer clips were made of 7075-T6 clad aluminum alloy. The skins were joined by the lap joints. The joint was a typical three-row configuration assembled using standard $\frac{3}{16}$-in. (4.8-mm)-diam, 100-deg countersunk-head rivets with rivet spacing of 1.07 in. (27.2 mm) in the tear strap region. The tear straps were hot bonded to the skins at each frame station. The outer and inner tear straps were overlapped above the lap joint. The detailed rivet distributions and detailed dimensions of panels, frames, stringers, and stringer clips can be found in Refs. 33 and 34.

A 5-in. (127-mm) initial saw cut was inserted along the upper rivet row in the outer skin. For the panel with MSD cracks, small 0.05-in. (1.27-mm) sawcuts were inserted in the outer skin after the rivet holes had been drilled but prior to the application of the fay sealant and rivet installation. The panels were subjected to pressure cycling until the length of a fatigue crack reached about two frame bays. The central frame was then cut, and the panels were loaded to failure statically. Rosette strain gauges were installed back to back on the skins and tear straps in the vicinity of the lap joint.

IV. Numerical Model

A. Modeling Strategy

In the present work all structural components including skins, stringers, and frames are modeled by displacement-based four-noded or five-noded quadrilateral shell elements.[18,35] Each node of the shell element has six degrees of freedom. To analyze the panel tests with reasonable computer resources and sufficient accuracy, a global-local approach is used. Figure 3 shows the typical finite

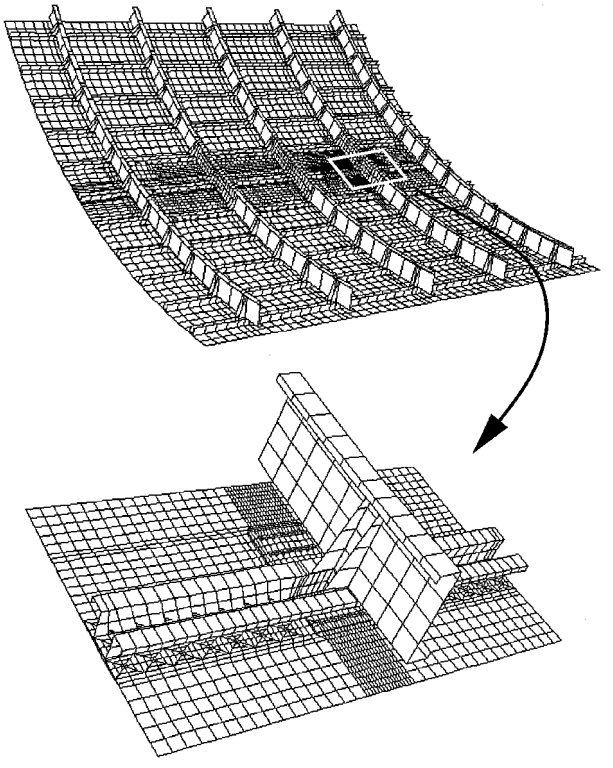

Fig. 3 Global and local finite element models.

element meshes for the two hierarchical modeling levels employed in the simulations. A 12-stringer-bay wide and 5-frame-bay long panel, which is about the size of the test panel, is modeled at the global level. A 1×1 bay stiffened panel is modeled at the local level. The local model differs from the global model in the finite element mesh density and the detailed geometric modeling of the cross-sectional shapes of stringers and frames.

Pressure loading is applied on all of the external skins. Symmetric boundary conditions are imposed on all of the boundary edges of the global model to simulate a cylinder-like fuselage structure. Uniform axial expansion is allowed at one longitudinal end. On this boundary edge an axial force equal to $(PR/2) \cdot L$ is assigned, where P is the applied pressure, R is the radius of the panel, and L is the arc length of the edge. The kinematic boundary conditions (displacements and rotations) applied along the boundaries of the local model are extracted from the global model results. In addition to these kinematic constraints, the local model is also subjected to internal pressure.

A piecewise linear idealization is used for the uniaxial stress-strain curves for 2024-T3 and 7075-T6 aluminum alloys (Figs. 4 and 5). Rivets are modeled by one-dimensional elastic-plastic fastener elements that connect finite element nodes in the upper and lower skins and tear straps. Each fastener element has six degrees of freedom, corresponding to extension, shearing, bending, and twisting of the rivet. The stiffness of each degree of freedom is defined by prescribing a piecewise linear force-deflection curve. The axial, flexural, and torsional stiffnesses of the fastener element are computed by assuming that the rivet behaves like a simple elastic rod with a diameter of $\frac{3}{16}$ in. (4.8 mm) based on elementary strength of materials: E, $1.05E04$ ksi; (72,390 MPa); L, 0.126 in. (3.2 mm); diameter, $\frac{3}{16}$ in. (4.8 mm); axial (EA/L), $2.30E03$ k (kilopound)/in. ($4.03E05$ kN/m); flexural (EI/L), 5.06 k/in. ($8.86E02$ kN/m); torsional (GJ/L), 3.80 k/in. ($6.65E02$ kN/m).

The elastic shear stiffness of the fastener element is computed by the following empirical relation developed by Swift[36]:

$$K_{\text{rivet}} = \frac{ED}{[A + C(D/t_1 + D/t_2)]} \tag{3}$$

where E is the elastic modulus of sheet material, D is the rivet diameter, t_1 and t_2 are thicknesses of joined sheets, and $A = 5.0$ and $C = 0.8$ for aluminum rivets. The initial shear yielding and ultimate shear strength of rivets are assumed to occur at load levels of 600 and 1080 lbf (2.7 and 4.8 N), respectively. A 80 and 95%

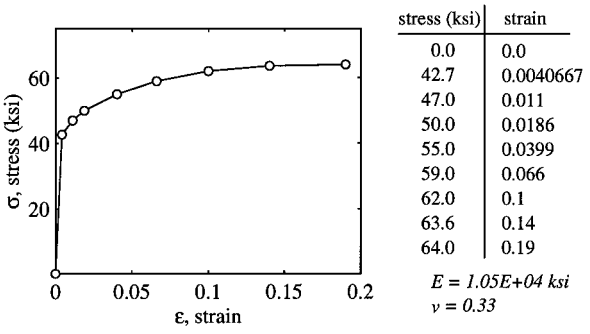

stress (ksi)	strain
0.0	0.0
42.7	0.0040667
47.0	0.011
50.0	0.0186
55.0	0.0399
59.0	0.066
62.0	0.1
63.6	0.14
64.0	0.19

E = 1.05E+04 ksi
v = 0.33

Fig. 4 Piecewise linear representation of the uniaxial stress-strain curve for 2024-T3 aluminum.

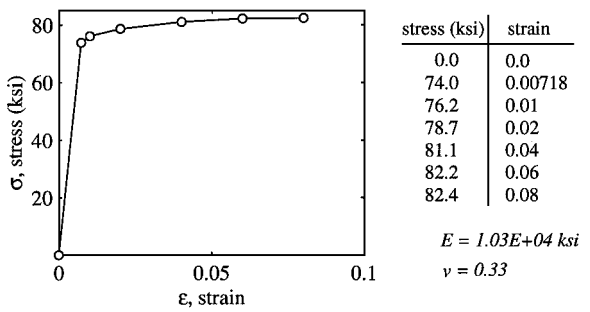

stress (ksi)	strain
0.0	0.0
74.0	0.00718
76.2	0.01
78.7	0.02
81.1	0.04
82.2	0.06
82.4	0.08

E = 1.03E+04 ksi
v = 0.33

Fig. 5 Piecewise linear representation of the uniaxial stress-strain curve for 7075-T6 aluminum.

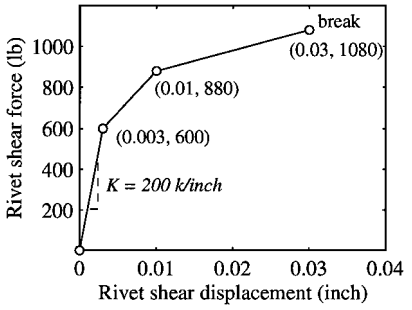

Fig. 6 Shear stiffness and strength of spring for rivet.

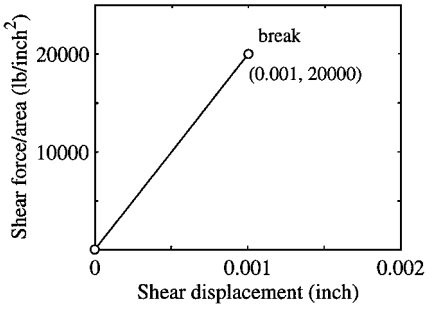

Fig. 7 Shear stiffness and strength of spring for adhesive.

reduction of the shear stiffness is assumed after the initial and second yielding. Once a rivet reaches its ultimate strength, it breaks and loses its load carrying capacity. The force-deflection curve shown in Fig. 6 for shearing is intended to represent, empirically, the net shear stiffness of a rivet-joined sheet connection, accounting for bearing deformations and local yielding around the rivet.[37]

The adhesive bond between skin and tear strap is also modeled with one-dimensional fastener elements. The shear stiffness is computed based on an effective area of the adhesive with[38]

$$K_{\text{adhesive}} = \frac{A_{\text{eff}}}{t_a/G_a + \left(\frac{3}{8}\right)(t_1/G + t_2/G)} \tag{4}$$

where A_{eff} is the bond area being lumped at the finite element nodal connection, G is the elastic shear modulus of sheet material, G_a is the elastic shear modulus of adhesive, t_1 and t_2 are the thicknesses of bonded sheets, and t_a is the thickness of adhesive bond. Because no adhesive tests were conducted, the material properties of adhesive G_a and t_a were obtained from the experimental results in Ref. 39. The maximum shear deflection is assumed to be 0.001 in. (0.025 mm). Similar to the rivet, once the fastener element for the adhesive reaches its ultimate strength it breaks and loses its load-carrying capacity. The force-deflection curve for shearing is shown in Fig. 7. The axial stiffness of the adhesive spring is derived from the shear stiffness by simply multiplying the ratio between elastic and shear modulus. The torsional and flexural stiffnesses of adhesive are assumed to be negligible.

Both geometric and material nonlinearities are used in the analysis at the global and local modeling levels. The global shell model captures the overall nonlinear response of the stiffened, curved, pressurized structure. The local shell model provides the detailed deformation and stress field near the crack tips to compute the fracture parameters (e.g., CTOA) that control crack growth.

B. Determination of CTOA$_c$

Flat-panel tests were conducted by the Boeing Commercial Airplane Group to obtain material properties for fatigue and fracture analysis of the curved fuselage panels. Four 48-in. (1220-mm)-wide, 80-in. (2030-mm)-long, 0.063-in. (1.6-mm)-thick middle crack tension (MT) specimens were tested. Three specimens were tested with guide plates to prevent out-of-plane buckling during crack growth. The flat-panel specimens were made from the same aluminum sheet used for the skin of the curved fuselage panels. A constant amplitude cyclic loading was applied to propagate an initial sawcut. After the fatigue crack growth a residual strength test was conducted under a

monotonically increasing load. The test matrix prior to the residual strength test is summarized in Table 1. Visual crack extension measurements were taken. Surface $CTOA_c$ was measured for Specimen 2024_FAA_TL3 during the residual strength test. Nine values were obtained, and the mean of the measured critical angles was about 5.5 deg with a scatter band about ±1.0 deg.

The value of $CTOA_c$ used in the residual strength analysis of the fuselage panels is determined by finding an angle within the scatter band of the $CTOA_c$ measurements that best correlates with the observed crack growth and residual strength of the coupon tests. The FRANC3D/STAGS program is used to simulate fracture behavior of the MT specimens. A finite element mesh that models a quarter of the specimen with a crack-tip element size of 0.04 in. (1 mm) and a half-plane-strain core height equal to 0.08 in. (2 mm) is shown in Fig. 8. The half core height is about the thickness of the specimen.

Figure 9 compares the predicted crack growth results to the experimental measurements. The $CTOA_c$ of 4.5 deg best correlates the predicted and measured residual strengths. However, it overpredicts crack growth at lower applied stress levels at the earlier stage of stable crack growth. The 5- and 5.5-deg critical angles give a better correlation for the earlier crack growth but overpredict the residual strength by 8.5 and 14.3%, respectively.

The discrepancy between predicted and measured crack growth at the earlier stage of tearing might relate to the residual plastic deformation left by the fatigue crack growth. This effectively increases the crack opening resistance during early stable crack growth.[40] Another factor that might affect crack growth and residual strength is the possible occurrence of short-wavelength out-of-plane buckling, although guide plates were used to prevent it. Such buckling in the MT specimen could reduce its crack growth resistance and residual strength.[41]

Table 1 Test matrix for MT specimens (after Ref. 33)

Specimen ID	Half initial crack, in.	Half final fatigue crack, in.	$\sigma_{fatigue}$, ksi	R
2024_FAA_TL3	2.0	8.0	8.0	0.1
2024_FAA_TL4	2.0	5.5	16.0	
	5.5	8.0	8.0	0.1
2024_FAA_TL5	5.0	12.0	12.0	0.1
2024_FAA_TL6	2.0	8.0	7.0	0.5

V. Strain Gauge Comparison

Strain gauge comparisons are made to verify predicted stress distributions at the onset of crack growth. Figure 10 shows the overall deformed structures for both the global and local models. Convergence studies are conducted to ensure accuracy of deformations and stress distributions.[15] Major results from the studies are summarized next:

1) For global models the predicted results converge quickly. The predicted membrane hoop stresses agree well with experimental measurements. The predicted bending hoop stresses are comparable to experimental measurements as one refines the finite element meshes (Fig. 11).

2) Predicted results from a local model with about the same mesh density as the corresponding region in the global model agree well with global model predictions and experimental measurements. The agreement ensures the transition accuracy in the hierarchical modeling.

3) Results with a much higher mesh density that is suitable for crack growth analysis disagree with the rest of the numerical predictions and experimental measurements. The discrepancy is thought to be related to the idealized representation of the two-noded fastener

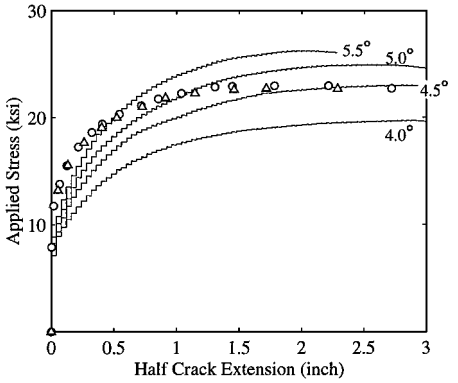

Fig. 9 Predicted applied stress vs crack growth for 48-in. (1220-mm)-wide MT specimen [half-plane-strain core height = 0.08 in. (2 mm)]: ○, 2024_FAA_TL3; △, 2024_FAA_TL4; and ——, predicted results.

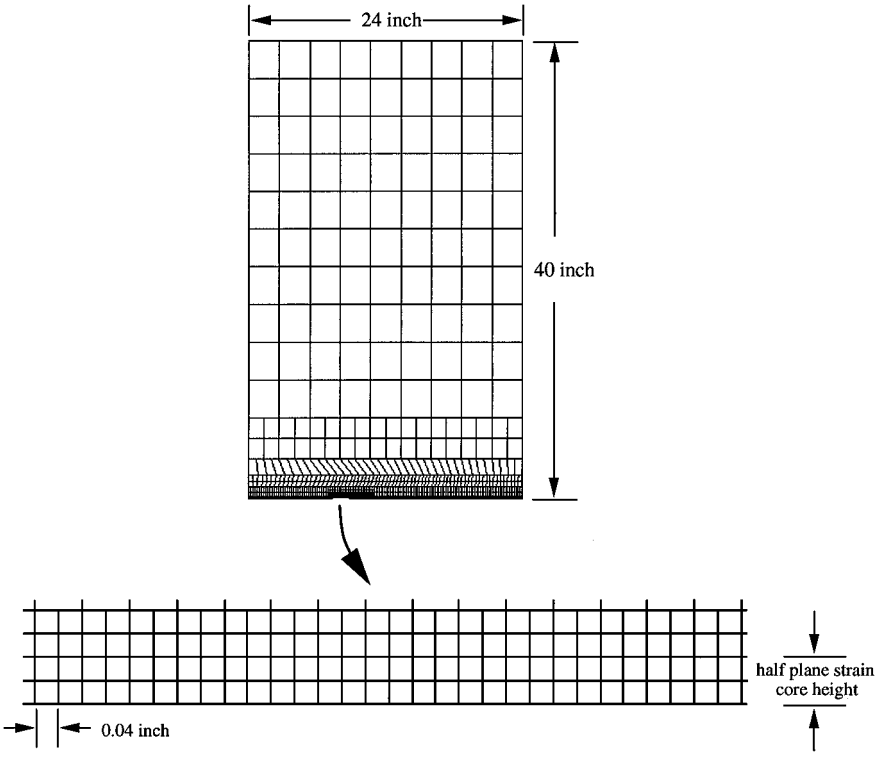

Fig. 8 Finite element mesh for one quarter of 48 × 80 in. (1220 × 2030 mm) MT specimen.

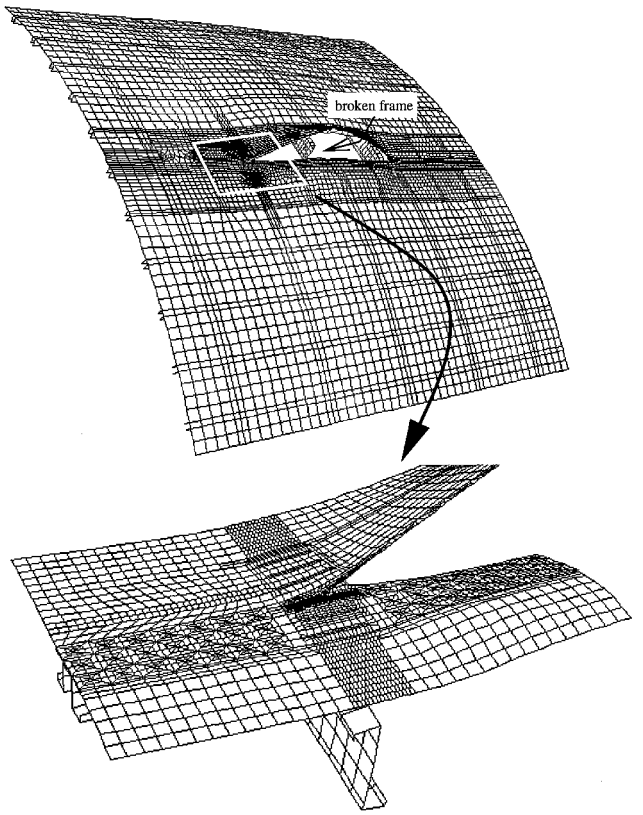

Fig. 10 Deformed structures of the validation example at global and local modeling levels [pressure = 9.4 psi (64.8 kPa), crack length = 38.2 in. (970 mm), magnification factor = 5.0].

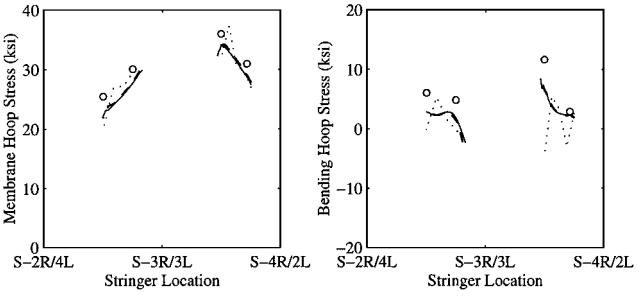

Fig. 11 Global convergence study: comparison between computed and measured hoop stresses (pressure = 9.4 psi (64.8 kPa); crack length = 38.2 in. (970 mm); frame cut; no MSD): ○, strain gauge measurement; · · · ·, global model (coarse mesh); – – –, global model (fine mesh); and ——, global model (finer mesh).

element for the rivet connection in the finite element model.[37,42] The single-point connection results in unrealistic distortion of the surrounding shell elements. The local distortion causes premature yielding of the shell elements and reduces the load transfer from sheet to rivet. This artificial distortion of the shell elements is discretization dependent (Ref. 42, pp. 318–327). Refining the mesh captures the local artificial distortion better, but makes the comparison to strain gauge readings worse.[37]

One approach to avoiding this artificial effect is to faithfully represent the geometry of the rivets and their interference with the sheets. This would considerably increase the required computational resources and might not be simple to implement in thin-shell elastic-plastic crack growth analysis.

A computationally more efficient approach adapted in the present study is to generate distributed connections between the two-noded fastener element and the surrounding shell elements.[37] The load distribution can be accomplished by defining rigid links, stiff spring elements, or a least-squares loading condition to connect the fastener node to the surrounding shell-element nodes. Care must be taken while defining the area in the shell elements over which the rivet

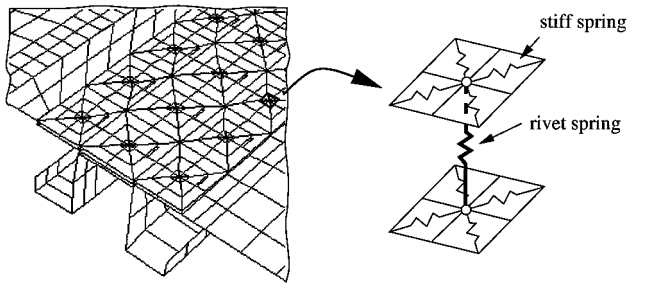

Fig. 12 Illustration of distributed connection that connects a fastener node to surrounding shell nodes.

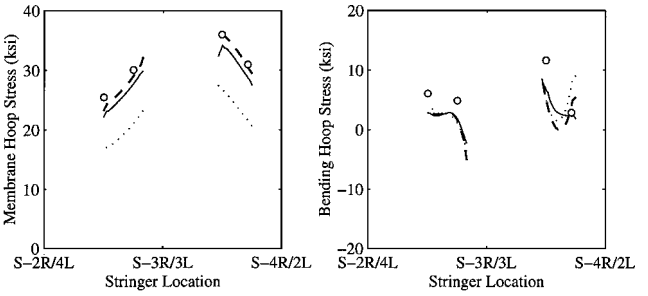

Fig. 13 Effects of distributed rivet connection: comparison between computed and measured hoop stresses [pressure = 9.4 psi (64.8 kPa), crack length = 38.2 in. (970 mm); frame cut; no MSD]: ○, strain gauge measurement; · · · ·, local model; – – –, local model with distributed connection; and ——, global model (finer mesh).

load is distributed. The area should be of the order of the rivet cross-sectional area because distributing the load over a larger area can inadvertently stiffen the shell elements. Figure 12 illustrates simulation of the distributed connection using stiff spring elements. The spring elements are assigned a stiffness an order of magnitude higher than that used for the rivet fastener elements to distribute the rivet load. Figure 13 shows the predicted hoop stress distributions with distributed connection simulations. A much better prediction is observed with the local mesh model.

The distributed connections might not be suitable to model the rivets located on the tearing path, for which the near-tip deformation is likely to be biased by such an arrangement. In our cases the tearing path is situated next to the rivet row connecting the skin/strap to the stringer (Fig. 14). When the cracked panel is subjected to pressure loading, we expect that the crack flank near the stringer is likely to experience much less deformation than the other. We thus apply a heuristic approach: only the shell elements on the less-deformed side of the crack are used to model the distributed rivet connection. Although this arrangement is not universally applicable, it works well in the present work; the unrealistic distortion caused by the single-point connection is eliminated while the undesired effects on the near-tip deformation from the distributed connections are avoided.

VI. Crack Growth and Residual Strength Analysis

Elastic-plastic crack growth and residual strength analyses are conducted using the local model. Both 4.5- and 5.5-deg critical angles computed at 0.04 in. (1 mm) behind the growing crack tip are used to investigate the sensitivity of $CTOA_c$ on stable crack growth and residual strength prediction. The 4.5-deg $CTOA_c$ is the angle that best correlates the predicted and observed residual strengths of the MT tests. The 5.5-deg angle is the mean from the surface $CTOA_c$ measurements in the MT tests. The plane-strain core height is 0.16 in. (4 mm) along the prescribed tearing path.

Figure 15 shows predicted results from the first attempt for stable crack growth analyses. The change of the $CTOA_c$ from 4.5 to 5.5 deg increases predicted residual strength by about 33 and 22% for the cases without and with MSD cracks, respectively.

Although analysis results in Fig. 15 clearly demonstrate the loss of residual strength as a result of the presence of MSD, all of the

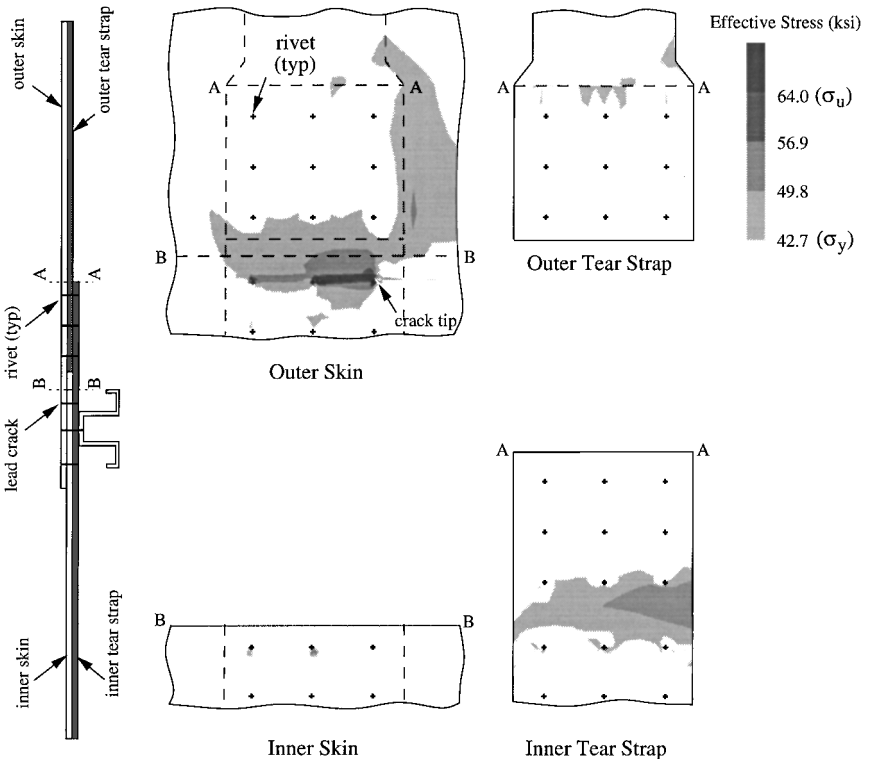

Fig. 14 Predicted effective stress distribution [pressure = 9.86 psi (68.0 kPa), da = 0.5 in. (12.7 mm), CTOA$_c$ = 5.5 deg].

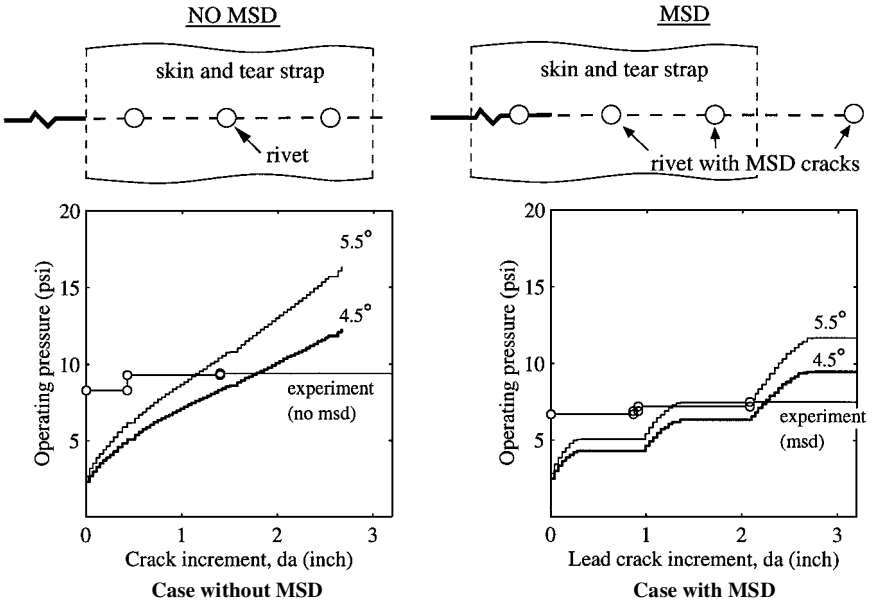

Fig. 15 Comparison between the predicted stable crack growth and experimental measurements.

predicted results underestimate the pressure loading to initiate the stable crack growth and overestimate the residual strength.

The much lower-predicted pressure for tearing initiation is likely caused by residual plastic deformation left by the fatigue crack growth. A possible cause for the lower residual strengths observed in the test might be related to the occurrence of tear strap failure. Both effects are discussed next.

A. Residual Plastic Deformation Effects

The test panels were subjected to pressure cycling prior to the residual strength test. To incorporate the residual plastic deformations caused by the cyclic loading, the residual strength analyses are reperformed using an elastic-plastic cyclic loading simulation suggested by Newman.[43] The procedure consists of the following steps:

Step 1: Close an appropriate length of fatigue crack.

Step 2: Load the fuselage model up to the maximum pressure loading conducted in fatigue tests.

Step 3: Release the crack-tip node and unload the model.

Step 4: Repeat steps 2 and 3 until the crack tip reaches the initial position for stable tearing.

This procedure implies that the fatigue crack only propagates at the maximum pressure during the cyclic loading simulation. For Mode I-only deformations under constant-amplitude load cycling, crack surfaces close at a positive applied load (i.e., step 3). The contact stresses cause the material to yield in compression. However, crack face contact and compressive yielding are ignored in the current simulations.

In subsequent analyses the fuselage model is brought to the operating pressure level during fatigue tests without allowing the crack to advance. The crack is then allowed to advance one element, and the load is returned to zero. Figure 16 plots results for a 0.32-in. (8-mm) length (eight elements) of fatigue crack closure used in the analysis for the case without MSD cracks. After two cycles of simulations, we observe that the crack-opening and crack-closure pressure have

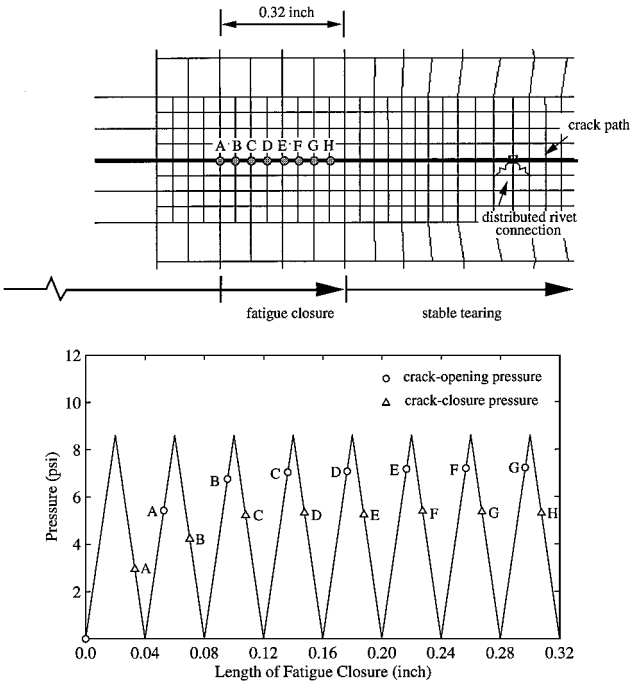

Fig. 16 Predicted crack-opening and crack-closure pressure under cyclic loading [cyclic pressure = 8.6 psi (59.3 kPa), no MSD].

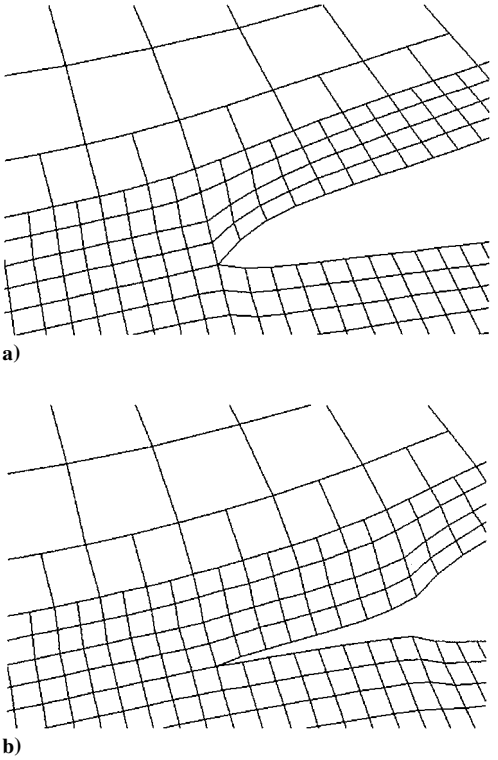

Fig. 17 Predicted crack opening profiles of outer skin at initial tearing crack tip: a) case without fatigue crack closure and b) case with 0.32-in. (8-mm) fatigue crack closure (no stable crack growth, magnification factor = 2.0).

stabilized. This implies that the residual plastic deformations caused by the cyclic loading are satiated in the model. We also performed several analyses with various lengths of fatigue crack closure; our numerical results suggest a 0.08-in. (2-mm) length (two elements) of fatigue crack closure is sufficient to model the residual plastic deformation effects.

Figure 17 shows two predicted crack opening profiles with and without fatigue crack closure effect when the pressure loading reaches 8.6 psi (59.3 kPa) (no growth). The effects of residual plastic deformations on the crack opening profile and consequently, the CTOA prediction, are clearly observed.

Table 2 Predicted and observed loading for tearing initiation

Case	Predicted, psi (6.89 kPa) $CTOA_c = 4.5$ deg	Predicted, psi (6.89 kPa) $CTOA_c = 5.5$ deg	Observed, psi
No MSD	2.3	2.7	8.3
No MSD [0.32-in. (8-mm) closure]	8.3	8.4	8.3
MSD	2.5	2.8	6.7
MSD [0.08-in. (2-mm) closure]	6.3	6.5	6.7

The 7.2-psi (49.6-kPa) crack-opening pressure shown in Fig. 16 seems to be too high in comparison with two-dimensional plane stress results[43] and laboratory observations.[44,45] This might be as a result of the lack of modeling of contact conditions when the crack closes. That is, the crack faces pass each other so that no compressive yielding is developed in the unloaded state. The compressive yielding stress would reduce residual tensile plastic deformation thus leading to a lower crack-opening pressure.[43] The crack face overlapping problem might be overcome by incorporating gap elements into shell analyses.

For the MSD case it is not clear to what extent we should model the residual plastic deformations at the MSD crack tips. In the present study we simply assign a 0.08-in. (2-mm) length of fatigue crack closure for both the lead and MSD cracks. During cyclic loading simulation, the lead and MSD crack tips are released simultaneously. Figure 18 shows the predicted crack-opening and crack-closure pressure for the MSD case. Further studies are needed to rationalize this approach for the MSD cracks.

Figure 19 shows predicted stable crack growth incorporating the residual plastic deformation effects. Table 2 summarizes the predicted and observed starting pressure to initiate stable crack growth. The plasticity-induced residual deformations increase the initiation pressure by about 150 to 210%. The predicted crack initiation loads are within 6% of experimental measurements for the cases that incorporate prior plastic residual deformations caused by fatigue crack growth. However, the predicted residual strengths are still higher than those observed.

B. Effects of Tear Strap Failure

One possible cause for the lower residual strengths observed in the test is the occurrence of failure of other structural elements. Figure 14 shows the predicted effective stress distribution in the outer skin, inner skin, outer tear strap, and inner tear strap as the stable crack growth analysis reaches 9.86-psi (68.0-kPa) pressure loading for the case without MSD cracks. Net section yielding is clearly shown in the inner tear strap.

The breakage of the inner tear strap during the residual strength test was also hypothesized in Ref. 33. To further investigate this damage scenario, a tear strap with rivet holes is modeled. By taking the kinematic boundary conditions from the local fuselage model, a stress concentration around the holes is observed (Fig. 20). It is then postulated that the high stress concentration is likely to initiate new cracks from the rivet holes thus leading to breakage of the inner tear strap.

To incorporate the tear strap damage scenario into the crack growth analysis, the inner tear strap is cut prior to fatigue crack closure and stable crack growth analyses as illustrated in Fig. 21. Figure 22 shows the predicted stable crack growth and residual strength for the fuselage models with a broken inner tear strap. The predicted residual strength using 4.5-deg $CTOA_c$ is within 13% of the experimental observation for the case without MSD cracks and within 1% of the experimental observation for the case with MSD cracks.

Additional damage scenarios are examined to study the effect of tear strap failure at various stages of stable crack growth. In these analyses we cut the inner tear strap at predetermined amounts of stable crack growth. Figure 23 shows the predicted stable crack growth and residual strength using 4.5-deg $CTOA_c$ for the fuselage

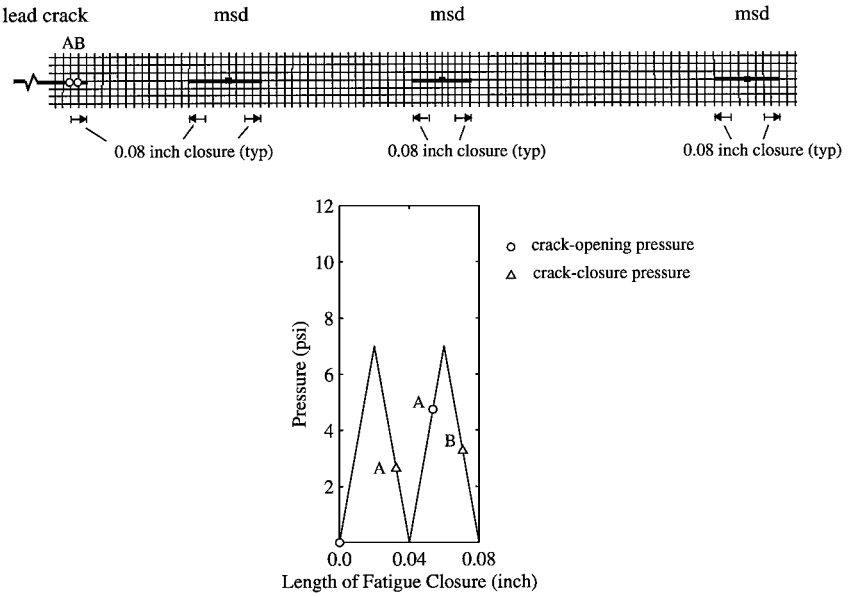

Fig. 18 Predicted crack-opening and crack-closure pressure under cyclic loading [cyclic pressure = 7.0 psi (48.3 kPa), MSD].

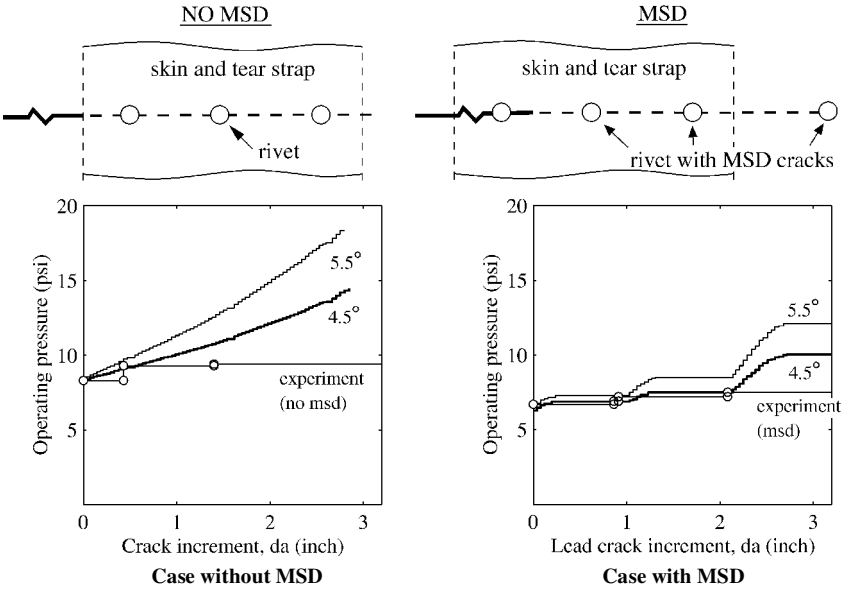

Fig. 19 Comparison between predicted stable crack growth with residual plastic deformation effects and experimental measurements.

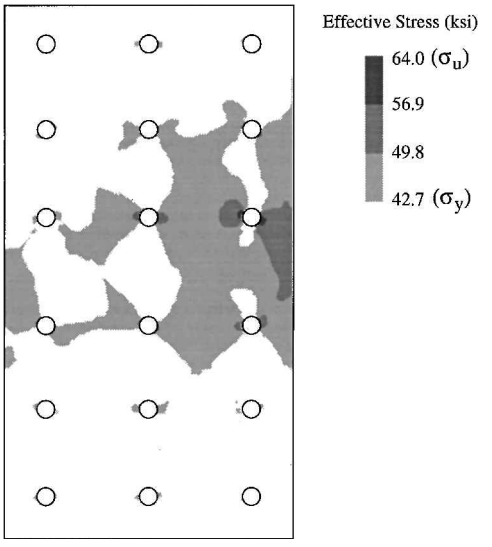

Fig. 20 Predicted effective stress distribution of inner tear strap with rivet holes [pressure = 9.86 psi (68.0 kPa), da = 0.5 in. (12.7 mm), $CTOA_c$ = 5.5 deg].

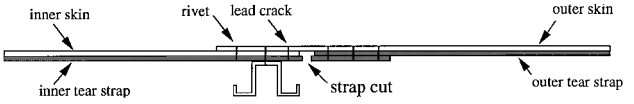

Fig. 21 Illustration of broken inner tear strap.

models without MSD cracks. For comparison, the predicted results with an intact tear strap shown in Fig. 19 are also plotted. The influence of the tear strap failure on residual strength prediction is again observed. The occurrence of the tear strap failure at various stages of stable crack growth affects the predicted crack growth resistance, but this scenario has a very mild influence on residual strength prediction.

The difference between predicted and observed residual strengths for the case without MSD cracks might be caused by excess residual plastic deformations modeled in the simulations. One way to reduce the plastic wake is to grow the crack at one-half the actual fatigue load. The corresponding crack-opening pressure with 0.32 in. (8 mm) of fatigue crack closure for the case without MSD is 3.2 psi (22.1 kPa). This, in conjunction with the tear strap damage scenario and 4.5-deg $CTOA_c$, predicts 9.34 psi residual strength for the case without MSD (Fig. 24). The result is within 1% of the experimental observation. However, the crack tearing now initiates at loads

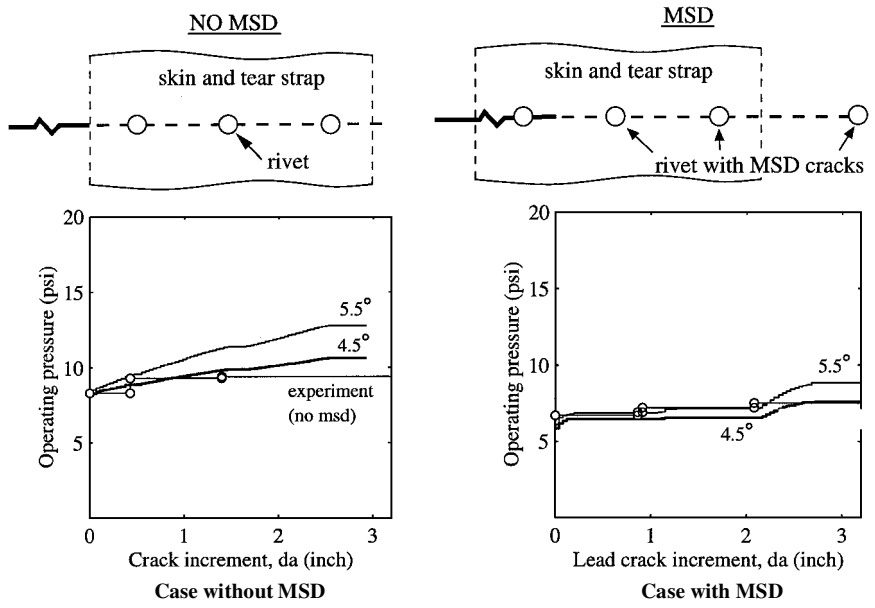

Fig. 22 Comparison between predicted stable crack growth with broken tear strap and experimental measurements.

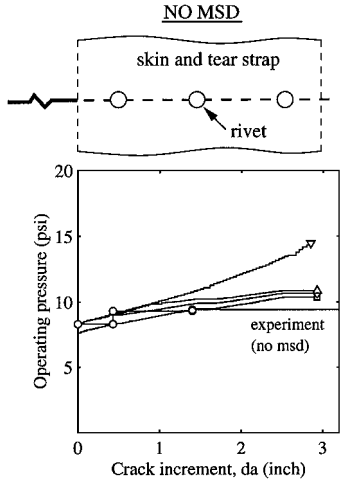

Fig. 23 Comparison between predicted results with tear strap failure at various stages during stable crack growth and experimental measurements (no MSD, $CTOA_c$ = 4.5 deg): ▽, intact tear strap; △, tear strap failure at da = 0.97 in.; ◇, tear strap failure at da = 0.43 in. (10.9 mm); and □, tear strap failure at da = 0.

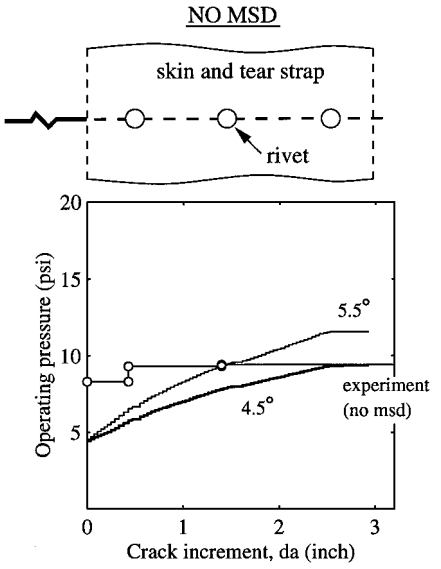

Fig. 24 Comparison between predicted stable crack growth and experimental measurements (broken tear strap, reduced plastic wake, no MSD).

much lower than those seen in the experiment, indicating that this correlation might only be coincidental.

VII. Conclusions

This paper presents a study on ductile tearing simulation and residual strength prediction of aircraft fuselages using the CTOA fracture criterion and elastic-plastic thin-shell finite element analysis. A generic wide-body fuselage panel is used to validate the analysis methodology. The major findings of this study are as follows:

1) The distributed connection for the rivet load transfer is crucial for a finite element model with a high mesh density to predict accurately the local stress distribution.

2) The occurrence of small MSD cracks substantially reduces the residual strength of pressurized fuselages. The reduction in the predicted residual strength caused by MSD varies from 28 to 47%. A difference of 20% was observed in the tests.

3) The residual strength prediction is sensitive to changes in $CTOA_c$. Altering the $CTOA_c$ from 4.5 to 5.5 deg changes the predicted residual strength by 17 to 33% for the case without MSD cracks. It changes the predicted residual strength by 12–22% for the case with MSD.

4) The residual plastic deformation or the plastic wake from fatigue crack growth has a strong effect on stable crack initiation and a mild effect on residual strength prediction. For crack growth initiation it is essential to incorporate the plastic wake from the fatigue crack growth to predict accurately the tearing initiation. Neglecting plastic wake effects leads to erroneous predictions of early stable crack growth. For residual strength analysis the plastic wake increases the predicted residual strength by 3–9%.

5) The breakage of the inner tear strap, a type of multiple-element damage, is crucial to residual strength prediction. The occurrence of the broken tear strap reduces the predicted residual strength by 24–30%.

Acknowledgments

This work was performed with support from the NASA Langley Aircraft Structural Integrity Program under Contract NAG-1-1184. Major funding for the development of FRANC3D was provided by the Northrop Grumman Corporation. We would like to thank James C. Newman Jr., David S. Dawicke, Charles E. Harris, Charles C. Rankin, Richard D. Young, Keith E. Wilkins, Michael L. Gruber, Paul Tan, Richard G. Pettit, and Bruce J. Carter for many helpful discussions. We also like to thank the referees for their helpful comments.

References

[1]U.S. Department of Transportation, "Damage Tolerance Assessment Handbook," Federal Aviation Administration, TR DOT-VNTSC-FAA-93-13.I, Atlantic City Airport, NJ, Oct. 1993.

[2]"Aloha Airlines, Flight 243. Boeing 737-200, N73711, Near Maui, Hawaii, April 28, 1988," National Transportation Safety Board, TR Aircraft Accident Report, NTSB/AAR-89/03, Washington, DC, June 1989.

[3]Harris, C. E., "NASA Airframe Structural Integrity Program," *Structural Integrity of Aging Airplanes*, Springer-Verlag, New York, 1991, pp. 141–152.

[4]Potyondy, D. O., Wawrzynek, P. A., and Ingraffea, A. R., "Discrete Crack Growth Analysis Methodology for Through Cracks in Pressurized Fuselage Structures," *International Journal for Numerical Methods in Engineering*, Vol. 38, No. 10, 1995, pp. 1611–1633.

[5]Bathe, K. J., *Finite Element Procedures*, Prentice–Hall, Upper Saddle River, NJ, 1996.

[6]Rice, J. R., "Mechanics of Quasi-Static Crack Growth," *IEEE Journal of Solid-State Circuits, Proceedings of the US National Congress of Applied Mechanics*, 1979, pp. 191–216.

[7]Newman, J. C., Jr., "An Evaluation of Fracture Analysis Methods," *Elastic-Plastic Fracture Mechanics Technology*, American Society for Testing and Materials, Philadelphia, 1985, pp. 5–96.

[8]Broek, D., *Elementary Engineering Fracture Mechanics*, Martinus—Nijhoff, Boston, 1986.

[9]Kanninen, M. F., and Popelar, C. H., *Advanced Fracture Mechanics*, Oxford Univ. Press, New York, 1985.

[10]Atluri, S. N., *Structural Integrity & Durability*, Tech Science Press, Forsyth, GA, 1997.

[11]Dawicke, D. S., and Newman, J. C., Jr., "Evaluation of Various Fracture Parameters for Predictions of Residual Strength in Sheets with Multi-Site Damage," *First Joint DoD/FAA/NASA Conference on Aging Aircraft*, Ogden, UT, 1997, pp. 1307–1326.

[12]Okada, H., and Atluri, S. N., "Further Studies on the Characteristics of the T_ϵ^* Integral: Plane Stress Stable Crack Propagation in Ductile Materials," *Computational Mechanics*, Vol. 23, No. 4, 1999, pp. 339–352.

[13]Newman, J. C., Jr., Dawicke, D. S., and Bigelow, C. A., "Finite-Element Analysis and Fracture Simulation in Thin-Sheet Aluminum Alloy," *Proceedings of the International Workshop on Structural Integrity of Aging Airplanes*, edited by S. N. Atluri, C. E. Harris, A. Hoggard, M. Miller, and S. G. Sampath, Atlanta Technology Publications, Atlanta, GA, 1992, pp. 167–186.

[14]Chen, C.-S., Wawrzynek, P. A., and Ingraffea, A. R., "Elastic-Plastic Crack Growth Simulation and Residual Strength Prediction of Thin Plates with Single and Multiple Cracks," *Fatigue and Fracture Mechanics: 29th Volume*, ASTM STP 1332, edited by T. L. Panontin and S. D. Sheppard, American Society for Testing and Materials, West Conshohocken, PA, 1999, pp. 97–113.

[15]Chen, C.-S., "Crack Growth Simulation and Residul Strength Prediction in Thin Shell Structures," Ph.D. Dissertation, School of Civil and Environmental Engineering, Cornell Univ., Ithaca, NY, Jan. 1999.

[16]Potyondy, D. O., "A Methodology for Simulation of Carvilinear Crack Growth in Pressurized Shells," Ph.D. Dissertation, School of Civil and Environmental Engineering, Cornell Univ., Ithaca, NY, Aug. 1993.

[17]Carter, B. J., Chen, C.-S., Wawrzynek, P. A., and Ingraffea, A. R., "A Topology-Based System for Modeling 3D Crack Growth in Solid and Shell Structures," *Proceedings of the Ninth International Congress on Fracture, ICF9*, Elsevier Science, New York, 1997, pp. 1923–1934.

[18]Rankin, C. C., Brogan, F. A., Loden, W. A., and Cabiness, H. D., "STAGS User Manual, Version 2.4," Lockheed Martin Missiles and Space Co., Inc., Advanced Technology Center, Palo Alto, CA, June 1997.

[19]Wells, A. A., "Unstable Crack Propagation in Metals: Cleavage and Fast Fracture," *Proceedings of the Cranfield Crack Propagation Symposium*, England, Cranfield, U.K., Vol. 1, 1961, pp. 210–230.

[20]Anderson, H., "Finite Element Representation of Stable Crack Growth," *Journal of the Mechanics and Physics of Solids*, Vol. 21, 1973, pp. 337–356.

[21]de Koning, A. U., "A Contribution to the Analysis of Quasi Static Crack Growth in Steel Materials," *Fracture 1977, Proceedings of the 4th International Conference on Fracture*, Vol. 3, edited by D. M. R. Taplin, Univ. of Waterloo Press, Waterloo, ON, Canada, 1977, pp. 25–31.

[22]Newman, J. C., Jr., "An Elastic-Plastic Finite Element Analysis of Crack Initiation, Stable Crack Growth, and Instability," *Fracture Mechanics: Fifteenth Symposium*, American Society for Testing and Materials, Philadelphia, 1984, pp. 93–117.

[23]Rice, J. R., and Sorensen, E. P., "Continuing Crack-Tip Deformation and Fracture for Plane-Strain Crack Growth in Elastic-Plastic Solids," *Journal of the Mechanics and Physics of Solids*, Vol. 26, 1978, pp. 163–186.

[24]Hom, C. L., and McMeeking, R. M., "Large Crack Tip Opening in Thin Elastic-Plastic Sheets" *International Journal of Fracture*, Vol. 45, 1990, pp. 103–122.

[25]Newman, J. C., Jr., Dawicke, D. S., Sutton, M. A., and Bigelow, C. A., "A Fracture Criterion for Widespread Cracking in Thin-Sheet Aluminum Alloys," *International Committee on Aeronautical Fatigue, 17th Symposium*, edited by A. F. Blom, Stockholm, 1993, pp. 443–468.

[26]Dawicke, D. S., Newman, J., Jr., and Bigelow, C. A., "Three-Dimensional CTOA and Constraint Effects During Stable Tearing in a Thin-Sheet Material," *Fracture Mechanics: 26th Volume*, American Society for Testing and Materials, Philadelphia, 1995, pp. 223–242.

[27]Thomason, P. F., *Ductile Fracture of Metals*, Pergamon, New York, 1990.

[28]Dawicke, D. S., Sutton, M. A., Newman, J. C., Jr., and Bigelow, C. A., "Measurement and Analysis of Critical CTOA for an Aluminum Alloy Sheet," *Fracture Mechanics: 25th Volume*, American Society for Testing and Materials, Philadelphia, 1995, pp. 358–379.

[29]Dawicke, D. S., "Residual Strength Predictions Using a Crack Tip Opening Angle Criterion," *Proceedings of the FAA-NASA Symposium on the Continued Airworthiness of Aircraft Structures*, edited by C. A. Bigelow, Atlanta, GA, 1996, pp. 555–566.

[30]Dawicke, D. S., and Newman, J. C., Jr., "Residual Strength Predictions for Multiple Site Damage Cracking Using a Three-Dimensional Analysis and a CTOA Criterion," *Fatigue and Fracture Mechanics: 29th Volume*, American Society for Testing and Materials, West Conshohocken, PA, 1999, pp. 815–829.

[31]Maclin, J. R., "Performance of Fuselage Pressure Structure," *1991 International Conference on Aging Aircraft and Structural Airworthiness*, edited by C. E. Harris, NASA Conference Publication 3160, 1991, pp. 67–74.

[32]Miller, M., Kaelber, K. N., and Worden, R. E., "Finite-Element Analysis of Pressure Vessel Panels," *Proceedings of the International Workshop on Structural Integrity of Aging Airplanes*, 1992, pp. 337–348.

[33]Gruber, M. L., Mazur, C. J., Wilkins, K. E., and Worden, R. E., "Investigation of Fuselage Structure Subject to Widespread Fatigue Damage," Federal Aviation Administration, TR DOT/FAA/AR-95/47, Washington, DC, Feb. 1996.

[34]Gruber, M. L., Wilkins, K. E., and Worden, R. E., "Investigation of Fuselage Structure Subject to Widespread Fatigue Damage," *Proceedigns of the FAA-NASA Symposium on the Continued Airworthiness of Aircraft Structures*, edited by C. A. Bigelow, Atlanta, GA, 1996, pp. 439–460.

[35]Rankin, C. C., and Brogan, F. A., "The Computational Structural Mechanics Testbed Structural Element Processor ES5: STAGS Shell Element," NASA CR-4358, May 1991.

[36]Swift, T., "Fracture Analysis of Stiffened Structure," *Damage Tolerance of Metallic Structures: Analysis Methods and Application*, American Society for Testing and Materials, Philadelphia, 1984, pp. 69–107.

[37]Young, R. D., Rose, C. A., Dávila, C. G., and Starnes, J. H., Jr., "Crack Growth and Residual Strength Characteristics of Selected Flat Stiffened Aluminum Panels," *First Joint DoD/FAA/NASA Conference on Aging Aircraft*, Ogden, UT, 1997, pp. 1765–1788.

[38]Singh, R., Park, J. H., and Atluri, S. N., "Growth of Multiple Cracks and Their Linkup in a Fuselage Lap Joint," *AIAA Journal*, Vol. 32, No. 11, 1994, pp. 2260–2268.

[39]Swift, T., "Fracture Analysis of Adhesively Bonded Cracked Panels," *Journal of Engineering Materials and Technology*, Vol. 100, 1978, pp. 10–15.

[40]Dawicke, D. S., Newman, J. C., Jr., Sutton, M. A., and Amstutz, B. E., "Influence of Crack History on the Stable Tearing Behavior of a Thin-Sheet Material with Multiple Cracks," *Proceedings of the FAA-NASA Sixth International Conference on the Continued Airworthiness of Aircraft Structures*, Atlantic City, NJ, 1994, pp. 193–212.

[41]Seshadri, B. R., and Newman, J. C., Jr., "Analysis of Buckling and Stable Tearing in Thin-Sheet Materials," *Fatigue and Fracture Mechanics: 29th Volume*, American Society for Testing and Materials, West Conshohocken, PA, 1999, pp. 114–134.

[42]Szabó, B., and Babuška, I., *Finite Element Analysis*, Wiley, New York, 1991.

[43]Newman, J. C., Jr., "A Finite-Element Analysis of Fatigue Crack Closure," *Mechanics of Crack Growth*, American Society for Testing and Materials, Philadelphia, 1976, pp. 281–301.

[44]Elber, W., "Fatigue Crack Closure Under Cyclic Tension," *Engineering Fracture Mechanics*, Vol. 2, 1970, pp. 37–45.

[45]Elber, W., "The Significance of Fatigue Crack Closure," *Damage Tolerance in Aircraft Structures*, American Society for Testing and Materials, Philadelphia, 1971, pp. 230–242.

E. Raymond
Associate Editor